

Ov3R: Open-Vocabulary Semantic 3D Reconstruction from RGB Videos

Ziren Gong
University of Bologna

Xiaohan Li
USTC

Fabio Tosi
University of Bologna

Jiawei Han
BIT

Stefano Mattoccia
University of Bologna

Jianfei Cai
Monash University

Matteo Poggi
University of Bologna

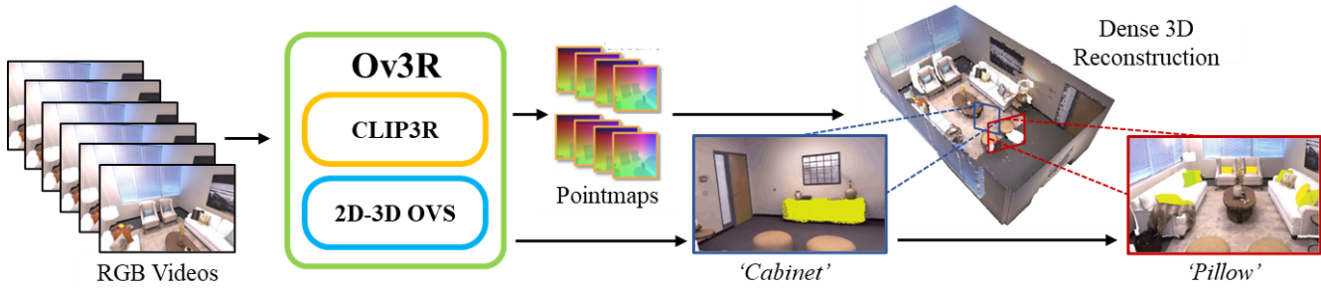


Figure 1. **Ov3R is an Open-Vocabulary Semantic 3D Reconstruction Framework.** It consists of two novel feed-forward modules, *CLIP3R* and *2D-3D OVS*, and excels in both 3D reconstruction and open-vocabulary 3D semantic segmentation.

Abstract

We present *Ov3R*, a novel framework for open-vocabulary semantic 3D reconstruction from RGB video streams, designed to advance Spatial AI. The system features two key components: *CLIP3R*, a CLIP-informed 3D reconstruction module that predicts dense point maps from overlapping clips alongside object-level semantics; and *2D-3D OVS*, a 2D-3D open-vocabulary semantic module that lifts 2D features into 3D by learning fused descriptors integrating spatial, geometric, and semantic cues. Unlike prior methods, *Ov3R* incorporates CLIP semantics directly into the reconstruction process, enabling globally consistent geometry and fine-grained semantic alignment. Our framework achieves state-of-the-art performance in both dense 3D reconstruction and open-vocabulary 3D segmentation — marking a step forward toward real-time, semantics-aware Spatial AI.

1. Introduction

Spatial AI systems [10] aim to understand both the geometry and semantics of the surrounding environment from images in real-time, enabling an embedded AI agent to navigate and interact with it effectively.

Dense 3D reconstruction lies at the core of these systems.

Over the decades, this task has taken various forms — from Structure-from-Motion (SfM) [30, 31, 42, 44] and Multi-View Stereo (MVS), typically performed offline, to Simultaneous Localization and Mapping (SLAM) [4, 13, 17, 47], which is executed online by autonomous agents and thus requires real-time processing. The latter flavor is the most suitable approach for developing Spatial AI systems, although it poses greater challenges compared to offline methods, as input images are collected incrementally rather than being available in advance — making the system susceptible to noise, motion blur, and cumulative drift over time.

In the last few years, SLAM has undergone a resurgence, fueled by advancements in related fields such as novel view synthesis [21, 35] and, more recently, the emergence of 3D reconstruction models [53] (3R), which have redefined the classical reconstruction paradigm by bypassing explicit camera pose estimation. The former has led to a family of SLAM methods, based on NeRF or 3DGS, yielding dense 3D reconstructions and accurate camera tracking, albeit with high computational cost due to the need for scene-specific training. The latter, in contrast, has resulted in the first 3R-based systems capable of real-time performance, though often at the expense of tracking accuracy, due to the absence of explicit pose estimation. In both directions, however, the semantic understanding of the surrounding environment has remained largely unexplored —

and where considered, it has been limited to simplified scenarios with a predefined set of classes [60, 61]. As a result, a significant gap between existing SLAM methods and envisioned Spatial AI systems still persists.

In parallel, with the emergence of CLIP [39], research on open-vocabulary 3D semantic understanding has surged. However, existing approaches largely rely on offline reconstruction pipelines [22, 36–38, 46, 48] or RGBD SLAM methods that require depth sensors [33], and therefore do not address the aforementioned gap.

In this paper, we introduce Ov3R, an open-vocabulary semantic 3D reconstruction framework that processes RGB-only video streams. Ov3R comprises two key components to achieve both accurate 3D reconstruction and semantic scene understanding: (i) CLIP3R, a CLIP-informed 3R model enriched with object-level CLIP features that encode the semantics of individual objects in the scene; and (ii) 2D–3D OVS, a module that integrates rich semantic information from various foundation models — CLIP3R itself, DINO and a distilled 3D-DINO encoder — to effectively segment the dense 3D reconstruction produced by CLIP3R. These two components are loosely coupled through the CLIP features, making Ov3R a modular framework capable of performing the two tasks either jointly or independently — e.g., running only 3D reconstruction when semantic understanding is not required or vice-versa.

Through extensive experiments on 3D reconstruction and open-vocabulary 3D segmentation, we demonstrate that Ov3R delivers high-quality dense scene reconstructions along with accurate open-vocabulary 3D semantic segmentation. Our main contributions are as follows:

- We present Ov3R, a novel framework that unifies cutting-edge 3R models and open-vocabulary 3D semantic segmentation - a bold step toward Spatial AI.
- We design CLIP3R, a CLIP-informed 3D reconstruction model that enforces semantic consistency across multi-view images and learns stronger semantic–geometric alignment.
- We propose 2D–3D OVS, a module that effectively lifts 2D CLIP descriptors into fused 2D–3D representations, enabling both spatial and geometric awareness to anchor language semantics and scene geometry.
- Ov3R achieves state-of-the-art performance in 3D reconstruction and open-vocabulary 3D segmentation.

2. Related Work

We identify two broad research areas relevant to our work.

2.1. 3D Reconstruction

Existing approaches for this task can be divided into offline, dense SLAM, and the recent 3R-based methods.

Offline Pipelines. This category includes strategies that assume the availability of a complete set of images before-

hand [30, 31, 42, 44], from which to process either camera parameters and 3D points via Structure from Motion (SfM) [1], or 3D points only through Multi-View Stereo (MVS) [50]. With the advent of NeRF [35] and 3DGS [21] for novel view synthesis, several derived frameworks [6–8, 18, 29] have been developed to achieve high-fidelity 3D reconstructions. However, offline processing does not fulfill the requirements of a Spatial AI system.

SLAM Systems. These approaches estimate the camera pose and the 3D structure of the environment during navigation – i.e., while images are being collected in real-time. Early hand-crafted works [3, 4, 12, 13, 47] focused mostly on camera tracking, while yielding sparse 3D reconstructions. More recently, the integration of novel views synthesis techniques (NeRF and 3DGS) into SLAM [49] has enabled both accurate and dense reconstructions, either assuming the availability of depth sensors [27, 28, 58] or not [25, 25, 58, 59, 62]. Although some of these frameworks have been enhanced with semantics understanding [60, 61], their scope is often limited to a fixed set of classes and lacks real-time capabilities.

3R-driven Models. DUST3R [53] pioneered the first end-to-end model for 3D reconstruction from two uncalibrated RGB images, predicting two pointmaps aligned to the same reference system, from which intrinsic and extrinsic camera parameters can also be derived. Several extensions of DUST3R target explicit features matching [24], single-image metric depth estimation [52], and dynamic scene reconstructions [57], although not achieving real-time performance. To address these limitations, Spann3R [51] introduces an incremental reconstruction approach to enable fast real-time operation. However, it rapidly accumulates drift errors due to the lack of global alignment and yields poor reconstruction accuracy. On the same track, SLAM3R [32] revisits SLAM by proposing a real-time 3D reconstruction method that does not require explicit pose estimation. Nonetheless, current 3R-based frameworks remain focused on detailed geometry reconstruction, disregarding higher-level scene understanding.

2.2. 3D Semantics

We can broadly classify 3D semantic segmentation approaches into closed-vocabulary and open-vocabulary ones.

Closed-Vocabulary Online Semantics. These methods predict per-pixel segmentation using pre-defined classes. SemanticFusion [34] pioneered per-pixel 3D semantic prediction from multi-view images. Recently, several semantic SLAM methods have been introduced to simultaneously reconstruct dense maps and semantics. NIS-SLAM [56] integrates semantics into tri-plane features to optimize both scene representation and semantic predictions. SGS-SLAM [26] and NEDS-SLAM [20] encode semantics into Gaussians and incrementally reconstruct scenes with a closed-set

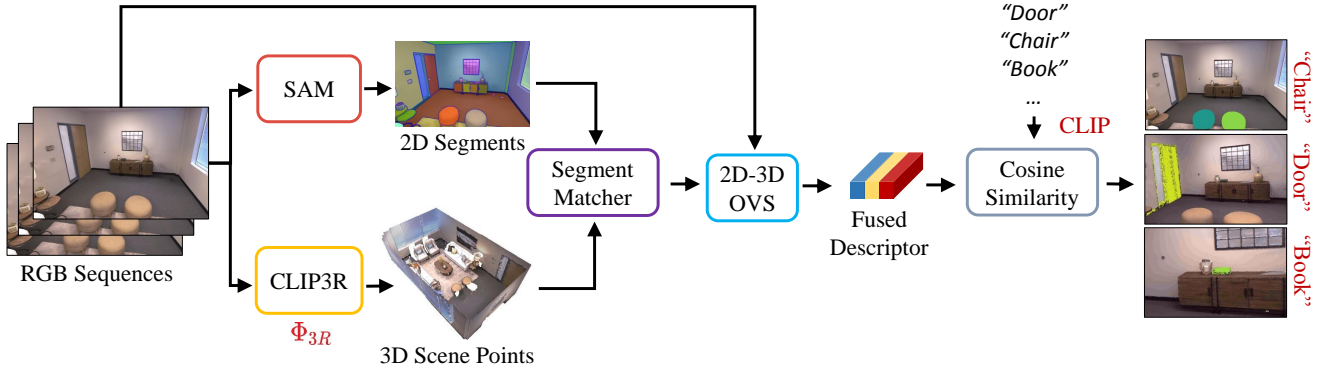


Figure 2. **Overview of Ov3R.** Given RGB-only videos, we first apply CLIP3R to produce scene points while SAM predicts 2D segments. Each 2D segment is matched to its corresponding 3D points to obtain 3D semantics. Next, the 2D-3D OVS extracts the fused 2D-3D descriptor to compute the cosine similarity with the text embeddings corresponding to a set of semantic classes.

segmentation. These methods achieve scene understanding by assuming a known set of 2D semantic annotations. However, relying on pre-defined semantic classes limits their applicability in real-world scenarios where novel object categories may appear.

3D Open-Vocabulary Offline Semantics. Most open-vocabulary semantic methods rely heavily on pre-processed 3D scene points as input. OpenScene [37] encodes per-pixel dense features in CLIP feature space and associates 2D dense features with known 3D scene points. Open3DIS [36] relies significantly on pre-processed 2D and 3D semantic instances to extract pointwise features. Unlike these approaches that require known 3D points, OpenNeRF [14] directly uses RGB images as input for NeRF and OpenSeg [16]. Similarly, HOV-SG [54] extracts 3D semantics and scene graph hierarchy from RGB-D sequences, relying heavily on feature pre-processing. Unlike the above offline methods, OVO [33] proposes the first online 3D open-vocabulary semantic mapping compatible with SLAM systems. It can extract and track 3D segments from RGB-D videos while encoding CLIP descriptors through a proposed CLIP merging strategy. However, it still requires depth information to be collected by an active sensor and explicit pose estimation from a SLAM system running concurrently. Besides, OVO computes CLIP descriptors solely from 2D images, overlooking the potential of 3D geometric information. In contrast, our Ov3R can extract 3D segments from RGB-only videos, not requiring explicit camera tracking.

3. Method

We now introduce Ov3R, whose overall architecture is depicted in Figure 2. It consists of two main components, highlighted in yellow and blue: (i) a CLIP-informed 3D-based model (CLIP3R) and (ii) a 2D-3D OVS module. CLIP3R produces dense scene points with semantic align-

ment in real-time, while 2D-3D OVS processes the semantic features predicted by the former for the downstream task of open-vocabulary 3D semantic segmentation. It enables Ov3R to reconstruct 3D semantic scenes while retaining the possibility to perform two tasks either jointly or independently.

3.1. CLIP3R

We introduce CLIP3R, a CLIP-informed 3D reconstruction model that integrates the rich semantic understanding embedded in CLIP features and enables open-vocabulary semantic segmentation as a downstream task thanks to the image-text alignment. It can be formalized as a model Φ_{3R} that processes multi-view RGB sequences $I_i^{(H \times W \times 3)}$ to predict dense point maps $P_i^{(H \times W \times 3)}$:

$$\Phi_{3R} \left(I_i^{(N \times H \times W \times 3)} \right) \rightarrow P_i^{(H \times W \times 3)}, i = 1, \dots, L \quad (1)$$

As shown in Figure 3, inspired by [32], CLIP3R deploys two main branches: an Image-to-Points (I2P, in yellow) model and a Local-to-World (L2W, in green) model.

1) The former is a ViT, inspired by DUS3R, running over a local window of images to predict a pointmap aligned to the reference system of the central frame (i.e., the keyframe). This is achieved by processing images with a shared encoder E_{img} and two decoders D_{key} and D_{sup} for the keyframe and remaining images, respectively. Notably, no explicit camera pose estimation is performed, which in turn can be derived from the pointmap as a byproduct.

2) The latter, instead, processes the local pointmaps and aligns them to the scene-level reconstruction. It employs a pointmap encoder E_{pts} , a registration decoder D_{reg} , and a scene decoder D_{sce} , sharing the same structure as the encoder and decoder used by I2P. It identifies correlated keyframes using a reservoir and retrieval strategy [32] and processes them to predict global scene points \hat{P}_i .

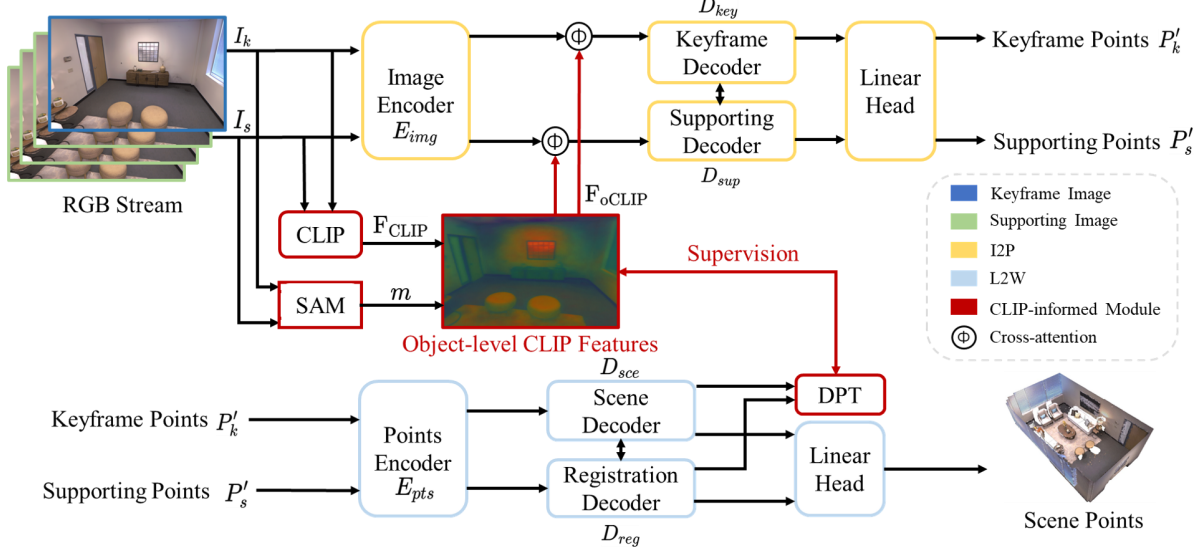


Figure 3. **CLIP3R Overview.** I2P integrates object-level CLIP features with visual embeddings to predict local pointmaps. L2W then aligns these local pointmaps to global scene coordinates while predicting object-level CLIP3R features with a DPT head in scene space.

Both branches, however, lack high-level reasoning about scene semantics, which we address through integration of CLIP features and CLIP-semantic supervision, to learn stronger semantic-geometric relationships and consistency.

Object-level CLIP3R features. Although rich in semantics, CLIP embeddings are image-level features and therefore fail at modeling the fine-grained semantics of individual objects in the scene [63]. To overcome this limitation, we extract object-level CLIP3R features $\mathbf{F}_{\text{oCLIP}}^{(H \times W \times D)}$ in place of vanilla CLIP features. This is achieved by first obtaining M object masks $m^{(H \times W \times 1)}$ using the Segment Anything Model (SAM) [23]. We then create M masked images and process them to extract CLIP patch embeddings, which are averaged and upsampled to $\mathbf{F}_{\text{CLIP}}^{(H \times W \times D)}$ to match the image resolution. Finally, the object-level features $\mathbf{F}_{\text{oCLIP}}^{(H \times W \times D)}$ are obtained by combining the individual CLIP features obtained from the M masked images within a single features map as:

$$\mathbf{F}_{\text{oCLIP}}^{(H \times W \times D)} = \sum_{i=0}^M m_i^{(H \times W \times 1)} \cdot \mathbf{F}_{\text{CLIP}_i}^{(H \times W \times D)} \quad (2)$$

These finer-level features are then integrated into CLIP3R, both in I2P and L2W branches in different ways.

CLIP-informed I2P. To predict local pointmaps, the I2P branch extracts visual tokens $\mathbf{F}_{\text{ViT}}^{(T \times d)}$ from each frame in the processed window through ViT blocks [11]. To enrich I2P with knowledge from CLIP, we concurrently extract object-level CLIP3R features and tokenize them into $\mathbf{F}_{\text{oCLIP}}^{(T \times d)}$. Then, $\mathbf{F}_{\text{oCLIP}}$ and \mathbf{F}_{ViT} are processed through cross-attention to obtain the fused features \mathbf{F}_{fuse} , which are

added to \mathbf{F}_{ViT} . The encoding process is denoted as:

$$\mathbf{F}_{\text{fuse}} = \mathbf{F}_{\text{ViT}} + \text{softmax}\left(\frac{\mathbf{F}_{\text{ViT}} \cdot \mathbf{F}_{\text{oCLIP}}^T}{\sqrt{d}}\right) \cdot \mathbf{F}_{\text{oCLIP}} \quad (3)$$

where d denotes the feature dimension. These features are then processed by the keyframe decoder D_{key} and the supporting decoder D_{sup} from the original I2P. A linear head is applied to predict both scene points P'_i ($P'_k, P'_s \in P'_i$) and confidence map C . The revised I2P network is trained end-to-end through a confidence-aware loss over ground truth scene points:

$$\mathcal{L}_{\text{I2P}} = \sum_{i=1}^L M_i \cdot (C \cdot \left\| \frac{1}{z'} P'_i - \frac{1}{z} P_i \right\|_1 - \alpha \log C) \quad (4)$$

where L is the number of supporting frames, M_i are the masked points with ground truth values in P_i , z and z' are scale factors, and α controls the confidence-based regularization term.

CLIP-informed L2W. The L2W branch maintains its original structure but incorporates an additional prediction head for object-level CLIP3R features, we refer to as $\mathbf{F}_{\text{CLIP3R}}$. This head embeds fine-grained semantic knowledge directly into the final 3D reconstruction while enforcing semantic consistency across the scene. This head is implemented as a DPT [40], and the entire L2W branch is trained using two losses: \mathcal{L}_{L2W} and $\mathcal{L}_{\text{oCLIP}}$. The former is similar to the loss used to supervise I2P:

$$\mathcal{L}_{\text{L2W}} = \sum_{i=1}^L M_i \cdot (\hat{C} \cdot \left\| \hat{P}'_i - P_i \right\|_1 - \alpha \log \hat{C}) \quad (5)$$

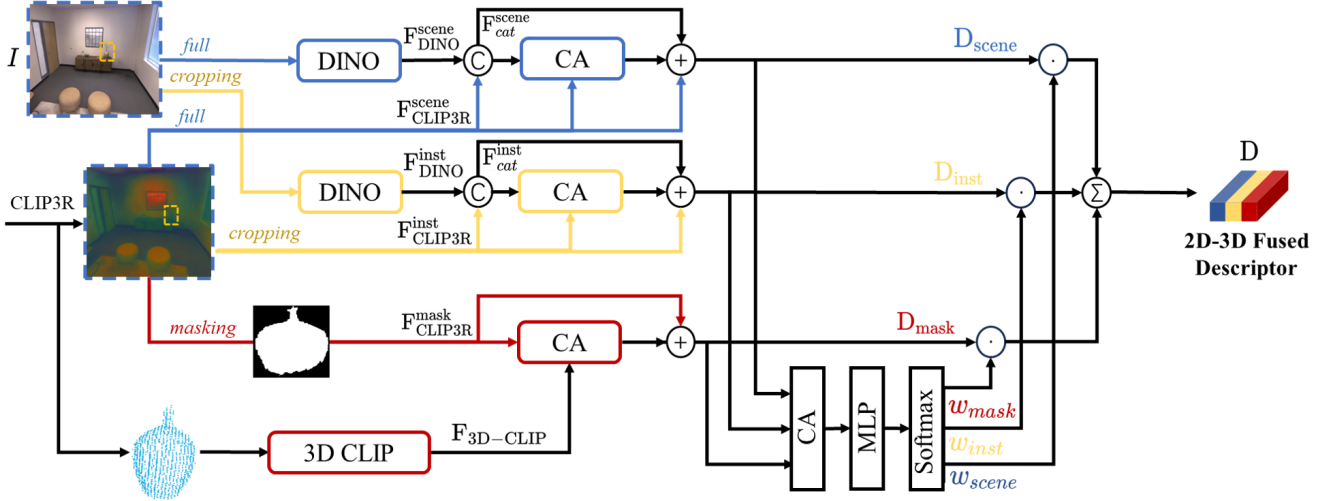


Figure 4. **2D-3D OVS Overview.** After matching 2D and 3D segments across images and pointmaps, CLIP3R, DINO, and 3D-CLIP features are combined into a 2D-3D fused descriptor, on top of which open-vocabulary semantic segmentation is performed. CLIP3R and DINO features are processed both at scene and instance levels. Meanwhile, 3D-CLIP features are extracted from masked 3D object points.

while the latter minimizes the feature distance between extracted $\mathbf{F}_{\text{oCLIP}}$ and predicted $\mathbf{F}_{\text{CLIP3R}}$ features:

$$\mathcal{L}_{\text{oCLIP}} = \|\mathbf{F}_{\text{CLIP3R}} - \mathbf{F}_{\text{oCLIP}}\|_1 \quad (6)$$

3.2. 2D-3D OVS

We now introduce the second core component of Ov3R, responsible for performing open-vocabulary 3D semantic segmentation over the 3D reconstruction produced by CLIP3R.

3D Segments Matching. We revise and improve the strategy from [33], replacing CLIP features with those predicted by CLIP3R: after predicting dense point maps for each frame, we project the 3D point map predicted by CLIP3R onto each keyframe to assign 2D segment labels to the matched 3D points, corresponding to the SAM-predicted masks already used by CLIP3R itself. After processing all 2D segments, 3D points sharing the same label are merged into coherent 3D segments. Although this strategy effectively selects individual semantic components in the scene, it relies solely on 2D information and lacks explicit semantic knowledge from the 3D geometry itself. To address this limitation, we introduce 2D-3D fused descriptors, obtained as follows.

2D-3D Fused Descriptors. CLIP3R features alone are insufficient to model semantics in 3D space, as they are learned from 2D CLIP features and thus lack fine-grained 3D structural information. On the same track, while DINO [5] features extract clear boundaries between inter-components, these lack knowledge about 3D geometry – which is, on the contrary, available from point features [19] extracted from 3D pointclouds. Therefore, we introduce a 2D-3D fused descriptor that combines these three complementary feature types extracted from i) CLIP3R, ii) DINO,

and iii) a 3D-CLIP encoder [19]:

i) To capture contextual information, we adopt the multi-level architecture by [54] and [33], as shown in Figure 4. From each keyframe, we leverage features predicted by CLIP3R (middle branch in the figure) at both scene-level (blue arrows in figure) and object instance-level (yellow arrows in figure), the latter by cropping the former according to 2D masks by SAM – referred to as $\mathbf{F}_{\text{CLIP3R}}^{\text{scene}}$ and $\mathbf{F}_{\text{CLIP3R}}^{\text{inst}}$;

ii) In parallel, DINO features are extracted (top branch in the figure) and again processed at both the scene and instance levels, similarly to CLIP3R features. These are referred to, respectively, as $\mathbf{F}_{\text{DINO}}^{\text{scene}}$ and $\mathbf{F}_{\text{DINO}}^{\text{inst}}$;

iii) Finally, instance-level 3D features are extracted from the point map after retaining only 3D points associated with the same object label (bottom branch in the figure). A 2D counterpart of the object-level features is retrieved from CLIP3R, by masking the cropped instance-level features according to 2D segmentation masks corresponding to the same object label (red arrow).

Therefore, 2D-aware features by DINO and CLIP3R are concatenated at both the scene and the instance levels independently (© in the figure), after projecting the former to the same feature dimension as the latter by a linear layer. Concatenated features are further processed by a linear layer

$$\mathbf{F}_{\text{cat}}^{\text{scene}} = \text{Linear}([\text{Linear}(\mathbf{F}_{\text{DINO}}^{\text{scene}}), \mathbf{F}_{\text{CLIP3R}}^{\text{scene}}]) \quad (7)$$

$$\mathbf{F}_{\text{cat}}^{\text{inst}} = \text{Linear}([\text{Linear}(\mathbf{F}_{\text{DINO}}^{\text{inst}}), \mathbf{F}_{\text{CLIP3R}}^{\text{inst}}]) \quad (8)$$

These features are cross-attended to original CLIP3R features at both levels independently (CA block in the figure). The resulting features are finally summed with the previous concatenated features and CLIP3R features (⊕ in the figure).

Method	Room0 Acc. / Comp.	Room1 Acc. / Comp.	Room2 Acc. / Comp.	Office0 Acc. / Comp.	Office1 Acc. / Comp.	Office2 Acc. / Comp.	Office3 Acc. / Comp.	Office4 Acc. / Comp.	Average Acc. / Comp.	ATE RMSE	FPS
DUSt3R	3.47 / 2.50	2.53 / 1.86	2.95 / 1.76	4.92 / 3.51	3.09 / 2.21	4.01 / 3.10	3.27 / 2.25	3.66 / 2.61	3.49 / 2.48	4.76	<1
MASt3R	4.01 / 4.10	3.61 / 3.25	3.13 / 2.15	2.57 / 1.63	12.85 / 8.13	3.13 / 1.99	4.67 / 3.15	3.69 / 2.47	4.71 / 3.36	1.67	<<1
NICER-SLAM	2.53 / 3.04	3.93 / 4.10	3.40 / 3.42	5.49 / 6.09	3.45 / 4.42	4.02 / 4.29	3.34 / 4.03	3.03 / 3.87	3.65 / 4.16	1.88	<<1
DROID-SLAM	12.18 / 8.96	8.35 / 6.07	3.26 / 16.01	3.01 / 16.19	2.39 / 16.20	5.66 / 15.56	4.49 / 9.73	4.65 / 9.63	5.50 / 12.29	0.33	20
DIM-SLAM	14.19 / 6.24	9.56 / 6.45	8.41 / 12.17	10.16 / 5.95	7.86 / 8.33	16.50 / 8.28	13.01 / 6.77	13.08 / 8.62	11.60 / 7.85	0.46	3
MGS-SLAM	-	-	-	-	-	-	-	-	7.51 / 3.64	0.32	0.6
GO-SLAM	-	-	-	-	-	-	-	-	3.81 / 4.79	0.39	8
Spann3R	9.75 / 12.94	15.51 / 12.94	7.28 / 8.50	5.46 / 18.75	5.24 / 16.64	9.33 / 11.80	16.00 / 9.03	13.97 / 16.02	10.32 / 13.33	32.79	>50
SLAM3R	3.19 / 2.40	3.12 / 2.34	2.72 / 2.00	4.28 / 2.60	3.17 / 2.34	3.84 / 2.78	3.90 / 3.16	4.32 / 3.36	3.57 / 2.62	6.61	24
Ov3R(Ours)	2.67 / 1.98	2.96 / 1.83	2.67 / 1.91	3.41 / 2.24	3.24 / 2.23	3.24 / 2.16	3.21 / 2.36	2.99 / 2.25	3.05 / 2.12	6.00	15

Table 1. **3D reconstruction and tracking results on Replica**. Methods are grouped into: 3R-driven methods with low FPS, SLAM-based approaches, and real-time 3R-driven frameworks. We highlight the **first**, **second**, and **third** best results.



Figure 5. **Qualitative results – Dense Pointmaps on Replica**. Compared to competing methods, Ov3R demonstrates superior completeness and geometric alignment, particularly visible in the reconstruction of **chairs (blue)** and **desks (yellow)**.

$$\mathbf{D}_{\text{scene}} = \mathbf{F}_{\text{CLIP3R}}^{\text{scene}} + \mathbf{F}_{\text{cat}}^{\text{scene}} + \text{softmax}\left(\frac{\mathbf{F}_{\text{CLIP3R}}^{\text{scene}} \cdot \mathbf{F}_{\text{cat}}^{\text{scene} T}}{\sqrt{d}}\right) \cdot \mathbf{F}_{\text{cat}}^{\text{scene}} \quad (9)$$

$$\mathbf{D}_{\text{inst}} = \mathbf{F}_{\text{CLIP3R}}^{\text{inst}} + \mathbf{F}_{\text{cat}}^{\text{inst}} + \text{softmax}\left(\frac{\mathbf{F}_{\text{CLIP3R}}^{\text{inst}} \cdot \mathbf{F}_{\text{cat}}^{\text{inst} T}}{\sqrt{d}}\right) \cdot \mathbf{F}_{\text{cat}}^{\text{inst}} \quad (10)$$

In parallel, we introduce a CLIP-like distilled 3D point encoder [19] to extract geometric features. This 3D encoder is pre-trained on triplets of point clouds, corresponding images, and text using natural language supervision. The 3D features obtained by this distilled encoder naturally align with the CLIP latent space. These 3D features are then processed by a linear layer and cross-attended with masked object-level CLIP3R features to learn semantic-geometric relationships, and finally summed to these latter again similarly to what done in the DINO branch.

$$\mathbf{D}_{\text{mask}} = \mathbf{F}_{\text{CLIP3R}}^{\text{mask}} + \text{softmax}\left(\frac{\mathbf{F}_{\text{CLIP3R}}^{\text{mask}} \cdot \mathbf{F}_{\text{3D-CLIP}}^T}{\sqrt{d}}\right) \cdot \mathbf{F}_{\text{3D-CLIP}} \quad (11)$$

Finally, we employ the weighted merging strategy from [33] to combine these three features from different levels:

$$\mathbf{D} = w_{\text{scene}} \odot \mathbf{D}_{\text{scene}} + w_{\text{inst}} \odot \mathbf{D}_{\text{inst}} + w_{\text{mask}} \odot \mathbf{D}_{\text{mask}} \quad (12)$$

where \mathbf{D} is our 2D-3D fused descriptor. \odot denotes the Hadamard product. The weights w_i are obtained by a shallow model comprising a cross-attention layer, an MLP, and a softmax layer. We pre-trained our 2D-3D fusion model by minimizing the sigmoid cosine similarity loss:

$$\mathcal{L}_{\text{sim}} = -\frac{1}{|B|} \sum_i^{|B|} \sum_j^{|B|} \log \left(\frac{1}{1 + e^{z_{ij}(-kd_i \cdot t_j + b)}} \right) \quad (13)$$

where B is a mini-batch containing pairs of 2D segments and semantic labels. z_{ij} is a binary label (1 or -1) indicating whether the segment and semantic label are paired. t_j is the text embedding encoded by CLIP. k and b are learnable bias and temperature parameters, respectively. At inference time, the similarity between fused descriptors and a set of text embeddings corresponding to semantic classes is computed: the class with the highest similarity is finally selected.

4. Experiments

Datasets. For the 3D reconstruction task, we follow [32] and train CLIP3R on ScanNet++ [55], Aria Synthetic Environments [2], and CO3D-v2 [41], which provide diverse scenarios and objects from both real-world and synthetic scenes. We evaluate 3D reconstruction performance on Replica [45] and 7Scenes [43]. For the open-vocabulary 3D segmentation task, we train the 2D-3D OVS module on ScanNet++ and evaluate it on Replica and ScanNetv2 [9], following [33]. Additionally, we report camera tracking results from CLIP3R on both Replica and 7Scenes.

Metrics. We adopt standard metrics including *Accuracy (cm)*, *completion (cm)* for 3D reconstruction, *Absolute Trajectory Error (ATE RMSE)* for tracking accuracy, and *Frame Per Second (FPS)* to assess efficiency. For open-vocabulary 3D segmentation, we use *mean Intersection Over Union (mIoU)* and *mean Accuracy (mAcc)* between the ground truth 3D labels and the labeled vertices of 3D meshes. Additionally, we evaluate label-frequency weighted metrics (f-mIoU and f-mAcc) for ScanNetv2.

Method	Chess Acc. / Comp.	Fire Acc. / Comp.	Heads Acc. / Comp.	Office Acc. / Comp.	Pumpkin Acc. / Comp.	RedKitchen Acc. / Comp.	Stairs Acc. / Comp.	Average Acc. / Comp.	ATE RMSE	FPS
DUS3R	2.26 / 2.13	1.04 / 1.50	1.66 / 0.98	4.62 / 4.74	1.73 / 2.43	1.95 / 2.36	3.37 / 10.75	2.19 / 3.24	8.02	<1
MAS3R	2.08 / 2.12	1.54 / 1.43	1.06 / 1.04	3.23 / 3.19	5.68 / 3.07	3.50 / 3.37	2.36 / 13.16	3.04 / 3.90	6.28	<<1
Spann3R	2.23 / 1.68	0.88 / 0.92	2.67 / 0.98	5.86 / 3.54	2.55 / 1.85	2.68 / 1.80	5.65 / 5.15	3.42 / 2.41	11.7	>50
SLAM3R	1.63 / 1.31	0.84 / 0.83	2.95 / 1.22	2.32 / 2.26	1.81 / 2.05	1.84 / 1.94	4.19 / 6.91	2.13 / 2.34	8.41	25
Ov3R(Ours)	1.53 / 1.26	0.79 / 0.76	2.41 / 0.99	1.95 / 1.93	1.66 / 1.89	1.63 / 1.82	3.88 / 5.95	1.98 / 2.08	7.71	17

Table 2. **3D reconstruction and tracking results on 7Scenes dataset.** The results are divided into two groups: 3R-driven methods with low FPS, and real-time 3R-driven frameworks.

Method	All mIoU / mAcc	Head mIoU / mAcc	Common mIoU / mAcc	Tail mIoU / mAcc
Geometry: GT				
OpenScene	15.9 / 24.6	31.7 / 44.8	14.5 / 22.6	1.5 / 6.3
OpenNeRF	20.4 / 31.7	35.4 / 46.2	20.1 / 31.3	5.8 / 17.6
HOV-SG	22.5 / 34.2	35.9 / 44.2	23.6 / 42.3	8.0 / 16.1
Open3DIS	25.6 / 38.7	49.7 / 64.4	22.1 / 42.4	4.9 / 9.4
OzV-mapping	7.8 / 13.9	19.3 / 27.5	4.0 / 6.7	0.1 / 7.5
OVO-mapping	26.5 / 35.8	41.0 / 52.3	21.1 / 31.8	17.6 / 23.2
Ov3R(Ours)	31.9 / 42.3	44.3 / 56.6	28.6 / 39.0	22.8 / 31.5
Geometry: CLIP3R				
OVO-CLIP3R	25.6 / 34.9	39.3 / 51.0	20.5 / 31.1	17.1 / 22.8
Ov3R(Ours)	30.4 / 41.2	42.8 / 54.9	26.8 / 38.0	21.7 / 30.8

Table 3. **Open-vocabulary 3D semantic segmentation results on Replica dataset.** On top: methods running on ground truth 3D reconstructions. At the bottom: methods running on CLIP3R reconstructions.

Implementation Details. Ov3R is trained on 4 NVIDIA A100 GPU, each with 64 GB of memory, while inference can be performed on a single 3090 NVIDIA GPU with 24 GB of memory. In CLIP3R, we set 24 encoder blocks and 12 decoder blocks with linear heads, setting the window length to $L = 5$ for initialization and $L = 11$ for subsequent incremental windows. The 2D-3D OVS model is trained for 15 epochs, with batch size 512. We use SAM 2.1 for 2D instance segmentation, SigLip ViT-SO400 for CLIP features, ViTS-16 for DINO features, and PointMLP-1024 for 3D point features.

4.1. 3D Reconstruction

We start by assessing the quality of 3D reconstructions produced by Ov3R against state-of-the-art methods.

Replica. Table 1 compares Ov3R against the state-of-the-art reconstruction methods on 8 scenes from Replica, including both SLAM-based and 3R-based approaches. Overall, Ov3R outperforms all state-of-the-art methods while maintaining up to 15 FPS processing speed. Although Spann3R achieves up to 50 FPS, it fails to provide accurate and complete 3D reconstructions, as shown in Figure 5. In contrast, Ov3R achieves consistently superior reconstructions compared to both Spann3R and SLAM3R.

7Scenes. Table 2 reports the evaluation on the 7Scenes dataset, carried out by uniformly sampling one-twentieth

Methods	ScanNet20				ScanNet200			
	mIoU	mAcc	f-mIoU	f-mAcc	mIoU	mAcc	f-mIoU	f-mAcc
Geometry: GT								
OpenScene	44.6	61.9	57.6	71.0	9.4	12.6	27.8	32.0
HOV-SG	34.4	51.1	47.3	61.8	11.2	18.7	27.7	37.6
Open3DIS	37.3	52.8	57.0	67.9	17.8	23.7	27.9	34.1
OVO-mapping	38.1	50.5	57.6	70.5	17.2	25.3	45.4	56.4
Ov3R(Ours)	43.6	57.8	65.0	79.4	19.4	28.5	50.8	61.6
Geometry: CLIP3R								
OVO-CLIP3R	32.6	44.2	48.9	64.8	14.1	21.5	38.0	51.2
Ov3R(Ours)	37.0	48.1	56.2	68.1	17.5	25.8	45.6	56.3

Table 4. **Open-vocabulary 3D semantic segmentation results on ScanNetv2.** On top: methods running on ground truth 3D reconstructions. At the bottom: methods running on CLIP3R reconstructions.

of the frames from each test sequence following [32]. As shown in the table, on average, Ov3R surpasses all of the baselines in both accuracy and completion, confirming the trends already highlighted on the Replica dataset.

4.2. Camera Tracking

Although 3R models do not explicitly estimate trajectories, camera poses can be derived from their predicted scene points. Following [53], we extract poses by running PnP-RANSAC [15] from the predicted 3D points, given the known camera intrinsics of each frame. Accordingly, we assess the tracking performance of Ov3R on the Replica and 7Scenes datasets. As shown in Table 1 and Table 2, Ov3R outperforms the other two real-time 3R-based frameworks, Spann3R and SLAM3R, narrowing the gap between this novel family of methods and the much slower dense SLAM systems.

4.3. Open-Vocabulary 3D Semantic Segmentation

We continue our evaluation by focusing on the open-vocabulary 3D semantic segmentation task. We conduct experiments under two different settings: segmentation performed on geometry reconstructed from (i) ground truth depth maps, simulating an offline setting, and (ii) RGB-only videos processed by CLIP3R.

Replica. We run experiments on the 8 standard scenes of Replica, annotated with 51 different semantic classes, and evaluate the results directly in 3D space rather than by projecting semantic masks onto 2D images [22]. Following



Figure 6. **Visualization of open-vocabulary 3D queries on the Replica.** We visualize two queries from “*Head*” and “*Common*” in *room0*. The similarities of queries are shown from *low* (blue) to *mid* (green), and *high* (yellow). OVO-mapping yields wrong “*Pillows*” and the missing “*Vase*”, while Open3DIS also produces wrong “*Pillows*” and low-similarity “*Vase*”.

	Acc.	Comp.	RMSE
(A) w/o CLIP-insert	3.31	2.35	6.46
(B) w/o CLIP head	3.20	2.21	6.32
Ov3R (all)	3.05	2.12	6.00

Table 5. **Ablation study of CLIP3R on Replica.** We study the impact of CLIP-insertion in I2P (CLIP-insert) and the CLIP-semantic supervision in L2W (CLIP head).

[14], these labels are divided into three categories (“*Head*”, “*Common*”, “*Tail*”) according to their frequency in the dataset. Thanks to its modular design, we compare Ov3R with both offline approaches and the recent online method, OVO [33]. In Table 3, Ov3R outperforms all baselines on *mIoU* and *mAcc* across *All* labels on average, achieving the best trade-off across all categories. Although Open3DIS achieves better performance on “*Head*” labels, it fails on less frequent objects. As shown in Figure 6, Ov3R accurately identifies the queried semantic classes, whereas OVO and Open3DIS produce inaccurate segmentation or miss objects entirely.

ScanNetv2. We continue the experiments on 5 scenes from ScanNetv2, using both the original (20) and extended (200) classes. Table 4 shows that Ov3R surpasses all baselines on the ScanNet200 dataset, demonstrating its generalization capability even with diverse and previously unseen class annotations. For the ScanNet20 dataset, Ov3R outperforms other methods in terms of *f-mIoU* and *f-mAcc* over ground truth reconstructions, while achieving comparable results to OpenScene in *mIoU* and *mAcc*. Notably, OpenScene performance significantly deteriorates when evaluated on a much larger set of classes. Consistently, Ov3R outperforms OVO in the online setting across both datasets.

4.4. Ablation Study

We conclude our experiments by assessing the impact of different sub-modules on 3D reconstruction and open-vocabulary 3D semantic segmentation.

	mIOU	mAcc	f-mIoU	f-mAcc
(C) w/o DINO	28.05	35.63	53.46	66.59
(D) w/o 3D encoder	28.46	36.20	52.81	65.38
Ov3R (all)	30.65	41.31	54.64	67.61

Table 6. **Ablation study of 2D-3D OV.** We report the advancement brought by different fusion strategies.

CLIP3R Component Analysis. We first assess the effects of our CLIP-informed strategy. As shown in Table 5, retaining only CLIP-semantic supervision (A) yields significant drops in both reconstruction accuracy and camera tracking, demonstrating the importance of CLIP cues in the reconstruction model. Moreover, removing the additional supervision (B) leads to consistently lower performance, confirming its key role in CLIP3R for 3D reconstruction.

2D-3D OVS Component Analysis. Table 6 shows that either CLIP descriptors fused with 3D features only (C) or those fused with DINO features only (D) lead to drops in accuracy. In contrast, our full 2D-3D OVS achieves the best performance, demonstrating that combining both 2D and 3D descriptors is crucial for accurate 3D segmentation.

5. Conclusion

We presented Ov3R, an open-vocabulary semantic 3D reconstruction framework. Compared to recent methods, Ov3R learns stronger semantic-geometric relationships and enforces semantic consistency through the proposed CLIP3R. Moreover, the introduced 2D-3D OVS enhances CLIP descriptors with spatial and geometric awareness. Our experiments demonstrate the superior accuracy and completeness of 3D reconstructions and 3D open-vocabulary semantic segmentation achieved by our approach.

Limitations and Future Work. Ov3R inherits one of the limitations of 3R models, i.e., the suboptimal accuracy of the retrieved camera poses. Future research will aim to overcome this limitation by integrating techniques from the

SLAM literature, such as global bundle adjustment.

References

- [1] Federica Arrigoni. A taxonomy of structure from motion methods. *arXiv preprint arXiv:2505.15814*, 2025. [2](#)
- [2] Armen Avetisyan, Christopher Xie, Henry Howard-Jenkins, Tsun-Yi Yang, Samir Aroudj, Suvam Patra, Fuyang Zhang, Duncan Frost, Luke Holland, Campbell Orme, et al. Scene-script: Reconstructing scenes with an autoregressive structured language model. In *European Conference on Computer Vision*, pages 247–263. Springer, 2024. [6](#)
- [3] Tim Bailey and Hugh Durrant-Whyte. Simultaneous localization and mapping (slam): Part ii. *IEEE robotics & automation magazine*, 13(3):108–117, 2006. [2](#)
- [4] Carlos Campos, Richard Elvira, Juan J Gómez Rodríguez, José MM Montiel, and Juan D Tardós. Orb-slam3: An accurate open-source library for visual, visual-inertial, and multimap slam. *IEEE transactions on robotics*, 37(6):1874–1890, 2021. [1](#), [2](#)
- [5] Mathilde Caron, Hugo Touvron, Ishan Misra, Hervé Jégou, Julien Mairal, Piotr Bojanowski, and Armand Joulin. Emerging properties in self-supervised vision transformers. In *Proceedings of the IEEE/CVF international conference on computer vision*, pages 9650–9660, 2021. [5](#)
- [6] Danpeng Chen, Hai Li, Weicai Ye, Yifan Wang, Weijian Xie, Shangjin Zhai, Nan Wang, Haomin Liu, Hujun Bao, and Guofeng Zhang. Pgsr: Planar-based gaussian splatting for efficient and high-fidelity surface reconstruction. *arXiv preprint arXiv:2406.06521*, 2024. [2](#)
- [7] Yuedong Chen, Haofei Xu, Chuanxia Zheng, Bohan Zhuang, Marc Pollefeys, Andreas Geiger, Tat-Jen Cham, and Jianfei Cai. Mvsplat: Efficient 3d gaussian splatting from sparse multi-view images. In *European Conference on Computer Vision*, pages 370–386. Springer, 2024.
- [8] Yuedong Chen, Chuanxia Zheng, Haofei Xu, Bohan Zhuang, Andrea Vedaldi, Tat-Jen Cham, and Jianfei Cai. Mvsplat360: Feed-forward 360 scene synthesis from sparse views. *Advances in Neural Information Processing Systems*, 37:107064–107086, 2024. [2](#)
- [9] Angela Dai, Angel X Chang, Manolis Savva, Maciej Halber, Thomas Funkhouser, and Matthias Nießner. Scannet: Richly-annotated 3d reconstructions of indoor scenes. In *Proceedings of the IEEE conference on computer vision and pattern recognition*, pages 5828–5839, 2017. [6](#)
- [10] Andrew J Davison. Futuremapping: The computational structure of spatial ai systems. *arXiv preprint arXiv:1803.11288*, 2018. [1](#)
- [11] Alexey Dosovitskiy, Lucas Beyer, Alexander Kolesnikov, Dirk Weissenborn, Xiaohua Zhai, Thomas Unterthiner, Mostafa Dehghani, Matthias Minderer, Georg Heigold, Sylvain Gelly, et al. An image is worth 16x16 words: Transformers for image recognition at scale. *arXiv preprint arXiv:2010.11929*, 2020. [4](#)
- [12] Hugh Durrant-Whyte and Tim Bailey. Simultaneous localization and mapping: part i. *IEEE robotics & automation magazine*, 13(2):99–110, 2006. [2](#)
- [13] Jakob Engel, Thomas Schöps, and Daniel Cremers. Lsd-slam: Large-scale direct monocular slam. In *European conference on computer vision*, pages 834–849. Springer, 2014. [1](#), [2](#)
- [14] Francis Engelmann, Fabian Manhardt, Michael Niemeyer, Keisuke Tateno, Marc Pollefeys, and Federico Tombari. Opennerf: open set 3d neural scene segmentation with pixel-wise features and rendered novel views. *arXiv preprint arXiv:2404.03650*, 2024. [3](#), [8](#)
- [15] Martin A. Fischler and Robert C. Bolles. Random sample consensus: A paradigm for model fitting with applications to image analysis and automated cartography. *Communications of the ACM*, 24(6):381–395, 1981. [7](#)
- [16] Golnaz Ghiasi, Xiuye Gu, Yin Cui, and Tsung-Yi Lin. Scaling open-vocabulary image segmentation with image-level labels. In *European conference on computer vision*, pages 540–557. Springer, 2022. [3](#)
- [17] Ziren Gong, Fabio Tosi, Youmin Zhang, Stefano Mattoccia, and Matteo Poggi. Hs-slam: Hybrid representation with structural supervision for improved dense slam. *arXiv preprint arXiv:2503.21778*, 2025. [1](#)
- [18] Antoine Guédon and Vincent Lepetit. Sugar: Surface-aligned gaussian splatting for efficient 3d mesh reconstruction and high-quality mesh rendering. In *Proceedings of the IEEE/CVF Conference on Computer Vision and Pattern Recognition*, pages 5354–5363, 2024. [2](#)
- [19] Deepthi Hegde, Jeya Maria Jose Valanarasu, and Vishal Patel. Clip goes 3d: Leveraging prompt tuning for language grounded 3d recognition. In *Proceedings of the IEEE/CVF International Conference on Computer Vision*, pages 2028–2038, 2023. [5](#), [6](#)
- [20] Yiming Ji, Yang Liu, Guanghu Xie, Boyu Ma, Zongwu Xie, and Hong Liu. Neds-slam: A neural explicit dense semantic slam framework using 3d gaussian splatting. *IEEE Robotics and Automation Letters*, 2024. [2](#)
- [21] Bernhard Kerbl, Georgios Kopanas, Thomas Leimkühler, and George Drettakis. 3d gaussian splatting for real-time radiance field rendering. *ACM Trans. Graph.*, 42(4):139–1, 2023. [1](#), [2](#)
- [22] Justin Kerr, Chung Min Kim, Ken Goldberg, Angjoo Kanazawa, and Matthew Tancik. Lerp: Language embedded radiance fields. In *Proceedings of the IEEE/CVF International Conference on Computer Vision*, pages 19729–19739, 2023. [2](#), [7](#)
- [23] Alexander Kirillov, Eric Mintun, Nikhila Ravi, Hanzi Mao, Chloe Rolland, Laura Gustafson, Tete Xiao, Spencer Whitehead, Alexander C Berg, Wan-Yen Lo, et al. Segment anything. In *Proceedings of the IEEE/CVF international conference on computer vision*, pages 4015–4026, 2023. [4](#)
- [24] Vincent Leroy, Yohann Cabon, and Jérôme Revaud. Grounding image matching in 3d with mast3r. In *European Conference on Computer Vision*, pages 71–91. Springer, 2024. [2](#)
- [25] Heng Li, Xiaodong Gu, Weihao Yuan, Luwei Yang, Zilong Dong, and Ping Tan. Dense rgb slam with neural implicit maps. *arXiv preprint arXiv:2301.08930*, 2023. [2](#)
- [26] Mingrui Li, Shuhong Liu, Heng Zhou, Guohao Zhu, Na Cheng, Tianchen Deng, and Hongyu Wang. Sgs-slam: Semantic gaussian splatting for neural dense slam. In *European*

- Conference on Computer Vision*, pages 163–179. Springer, 2024. 2
- [27] Xiaohan Li, Shiqi Lin, Meng Xu, Deyun Dai, and Jikai Wang. Po-slam: a novel monocular visual slam with points and objects. In *2021 4th International conference on artificial intelligence and big data (ICAIBD)*, pages 454–458. IEEE, 2021. 2
- [28] Xiaohan Li, Dong Liu, and Jun Wu. Cto-slam: contour tracking for object-level robust 4d slam. In *Proceedings of the AAAI Conference on Artificial Intelligence*, pages 10323–10331, 2024. 2
- [29] Zhaoshuo Li, Thomas Müller, Alex Evans, Russell H Taylor, Mathias Unberath, Ming-Yu Liu, and Chen-Hsuan Lin. Neuralangelo: High-fidelity neural surface reconstruction. In *Proceedings of the IEEE/CVF Conference on Computer Vision and Pattern Recognition*, pages 8456–8465, 2023. 2
- [30] Philipp Lindenberger, Paul-Edouard Sarlin, Viktor Larseron, and Marc Pollefeys. Pixel-perfect structure-from-motion with featuremetric refinement. In *Proceedings of the IEEE/CVF international conference on computer vision*, pages 5987–5997, 2021. 1, 2
- [31] Shaohui Liu, Yifan Yu, Rémi Pautrat, Marc Pollefeys, and Viktor Larsson. 3d line mapping revisited. In *Proceedings of the IEEE/CVF Conference on Computer Vision and Pattern Recognition*, pages 21445–21455, 2023. 1, 2
- [32] Yuzheng Liu, Siyan Dong, Shuzhe Wang, Yingda Yin, Yanchao Yang, Qingnan Fan, and Baoquan Chen. Slam3r: Real-time dense scene reconstruction from monocular rgb videos. In *Proceedings of the Computer Vision and Pattern Recognition Conference*, pages 16651–16662, 2025. 2, 3, 6, 7
- [33] Tomas Berriel Martins, Martin R Oswald, and Javier Civera. Ovo-slam: Open-vocabulary online simultaneous localization and mapping. *arXiv preprint arXiv:2411.15043*, 2024. 2, 3, 5, 6, 8
- [34] John McCormac, Ankur Handa, Andrew Davison, and Stefan Leutenegger. Semanticfusion: Dense 3d semantic mapping with convolutional neural networks. In *2017 IEEE International Conference on Robotics and automation (ICRA)*, pages 4628–4635. IEEE, 2017. 2
- [35] Ben Mildenhall, Pratul P Srinivasan, Matthew Tancik, Jonathan T Barron, Ravi Ramamoorthi, and Ren Ng. Nerf: Representing scenes as neural radiance fields for view synthesis. *Communications of the ACM*, 65(1):99–106, 2021. 1, 2
- [36] Phuc Nguyen, Tuan Duc Ngo, Evangelos Kalogerakis, Chuang Gan, Anh Tran, Cuong Pham, and Khoi Nguyen. Open3dis: Open-vocabulary 3d instance segmentation with 2d mask guidance. In *Proceedings of the IEEE/CVF Conference on Computer Vision and Pattern Recognition*, pages 4018–4028, 2024. 2, 3
- [37] Songyou Peng, Kyle Genova, Chiyu Jiang, Andrea Tagliasacchi, Marc Pollefeys, Thomas Funkhouser, et al. Openscene: 3d scene understanding with open vocabularies. In *Proceedings of the IEEE/CVF conference on computer vision and pattern recognition*, pages 815–824, 2023. 3
- [38] Minghan Qin, Wanhua Li, Jiawei Zhou, Haoqian Wang, and Hanspeter Pfister. Langsplat: 3d language gaussian splatting. In *Proceedings of the IEEE/CVF Conference on Computer Vision and Pattern Recognition*, pages 20051–20060, 2024. 2
- [39] Alec Radford, Jong Wook Kim, Chris Hallacy, Aditya Ramesh, Gabriel Goh, Sandhini Agarwal, Girish Sastry, Amanda Askell, Pamela Mishkin, Jack Clark, et al. Learning transferable visual models from natural language supervision. In *International conference on machine learning*, pages 8748–8763. PMLR, 2021. 2
- [40] René Ranftl, Alexey Bochkovskiy, and Vladlen Koltun. Vision transformers for dense prediction. In *Proceedings of the IEEE/CVF international conference on computer vision*, pages 12179–12188, 2021. 4
- [41] Jeremy Reizenstein, Roman Shapovalov, Philipp Henzler, Luca Sbordone, Patrick Labatut, and David Novotny. Common objects in 3d: Large-scale learning and evaluation of real-life 3d category reconstruction. In *Proceedings of the IEEE/CVF international conference on computer vision*, pages 10901–10911, 2021. 6
- [42] Johannes L Schonberger and Jan-Michael Frahm. Structure-from-motion revisited. In *Proceedings of the IEEE conference on computer vision and pattern recognition*, pages 4104–4113, 2016. 1, 2
- [43] Jamie Shotton, Ben Glocker, Christopher Zach, Shahram Izadi, Antonio Criminisi, and Andrew Fitzgibbon. Scene coordinate regression forests for camera relocalization in rgb-d images. In *Proceedings of the IEEE conference on computer vision and pattern recognition*, pages 2930–2937, 2013. 6
- [44] Noah Snavely, Steven M Seitz, and Richard Szeliski. Photo tourism: exploring photo collections in 3d. In *ACM siggraph 2006 papers*, pages 835–846. 2006. 1, 2
- [45] Julian Straub, Thomas Whelan, Lingni Ma, Yufan Chen, Erik Wijmans, Simon Green, Jakob J Engel, Raul Mur-Artal, Carl Ren, Shobhit Verma, et al. The replica dataset: A digital replica of indoor spaces. *arXiv preprint arXiv:1906.05797*, 2019. 6
- [46] Ayça Takmaz, Elisabetta Fedele, Robert W Sumner, Marc Pollefeys, Federico Tombari, and Francis Engelmann. Open-mask3d: Open-vocabulary 3d instance segmentation. *arXiv preprint arXiv:2306.13631*, 2023. 2
- [47] Zachary Teed and Jia Deng. Droid-slam: Deep visual slam for monocular, stereo, and rgb-d cameras. *Advances in neural information processing systems*, 34:16558–16569, 2021. 1, 2
- [48] Muer Tie, Julong Wei, Ke Wu, Zhengjun Wang, Shanshuai Yuan, Kaizhao Zhang, Jie Jia, Jieru Zhao, Zhongxue Gan, and Wenchao Ding. O 2 v-mapping: Online open-vocabulary mapping with neural implicit representation. In *European Conference on Computer Vision*, pages 318–333. Springer, 2024. 2
- [49] Fabio Tosi, Youmin Zhang, Ziren Gong, Erik Sandström, Stefano Mattoccia, Martin R Oswald, and Matteo Poggi. How nerfs and 3d gaussian splatting are reshaping slam: a survey. *arXiv preprint arXiv:2402.13255*, 4:1, 2024. 2
- [50] Fangjinhua Wang, Qingtian Zhu, Di Chang, Quankai Gao, Junlin Han, Tong Zhang, Richard Hartley, and Marc Pollefeys. Learning-based multi-view stereo: A survey. *arXiv preprint arXiv:2408.15235*, 2024. 2

- [51] Hengyi Wang and Lourdes Agapito. 3d reconstruction with spatial memory. *arXiv preprint arXiv:2408.16061*, 2024. 2
- [52] Ruicheng Wang, Sicheng Xu, Cassie Dai, Jianfeng Xiang, Yu Deng, Xin Tong, and Jiaolong Yang. Moge: Unlocking accurate monocular geometry estimation for open-domain images with optimal training supervision. In *Proceedings of the Computer Vision and Pattern Recognition Conference*, pages 5261–5271, 2025. 2
- [53] Shuzhe Wang, Vincent Leroy, Yohann Cabon, Boris Chidlovskii, and Jerome Revaud. Dust3r: Geometric 3d vision made easy. In *Proceedings of the IEEE/CVF Conference on Computer Vision and Pattern Recognition*, pages 20697–20709, 2024. 1, 2, 7
- [54] Abdelrhman Werby, Chenguang Huang, Martin Büchner, Abhinav Valada, and Wolfram Burgard. Hierarchical open-vocabulary 3d scene graphs for language-grounded robot navigation. In *First Workshop on Vision-Language Models for Navigation and Manipulation at ICRA 2024*, 2024. 3, 5
- [55] Chandan Yeshwanth, Yueh-Cheng Liu, Matthias Nießner, and Angela Dai. Scannet++: A high-fidelity dataset of 3d indoor scenes. In *Proceedings of the IEEE/CVF International Conference on Computer Vision*, pages 12–22, 2023. 6
- [56] Hongjia Zhai, Gan Huang, Qirui Hu, Guanglin Li, Hujun Bao, and Guofeng Zhang. Nis-slam: Neural implicit semantic rgb-d slam for 3d consistent scene understanding. *IEEE Transactions on Visualization and Computer Graphics*, 2024. 2
- [57] Junyi Zhang, Charles Herrmann, Junhwa Hur, Varun Jampani, Trevor Darrell, Forrester Cole, Deqing Sun, and Ming-Hsuan Yang. Monst3r: A simple approach for estimating geometry in the presence of motion. *arXiv preprint arXiv:2410.03825*, 2024. 2
- [58] Youmin Zhang, Fabio Tosi, Stefano Mattoccia, and Matteo Poggi. Go-slam: Global optimization for consistent 3d instant reconstruction. In *Proceedings of the IEEE/CVF International Conference on Computer Vision*, pages 3727–3737, 2023. 2
- [59] Pengcheng Zhu, Yaoming Zhuang, Baoquan Chen, Li Li, Chengdong Wu, and Zhanlin Liu. Mgs-slam: Monocular sparse tracking and gaussian mapping with depth smooth regularization. *IEEE Robotics and Automation Letters*, 2024. 2
- [60] Siting Zhu, Renjie Qin, Guangming Wang, Jiuming Liu, and Hesheng Wang. Semgauss-slam: Dense semantic gaussian splatting slam. *arXiv preprint arXiv:2403.07494*, 2024. 2
- [61] Siting Zhu, Guangming Wang, Hermann Blum, Jiuming Liu, Liang Song, Marc Pollefeys, and Hesheng Wang. Sni-slam: Semantic neural implicit slam. In *Proceedings of the IEEE/CVF Conference on Computer Vision and Pattern Recognition*, pages 21167–21177, 2024. 2
- [62] Zihan Zhu, Songyou Peng, Viktor Larsson, Zhaopeng Cui, Martin R Oswald, Andreas Geiger, and Marc Pollefeys. Nicer-slam: Neural implicit scene encoding for rgb slam. In *2024 International Conference on 3D Vision (3DV)*, pages 42–52. IEEE, 2024. 2
- [63] Xingxing Zuo, Pouya Samangouei, Yunwen Zhou, Yan Di, and Mingyang Li. Fmgs: Foundation model embedded 3d gaussian splatting for holistic 3d scene understanding. *International Journal of Computer Vision*, 133(2):611–627, 2025. 4